International Symposium on Solar Terrestrial Physics
ASI Conference Series, 2013, Vol. 10, pp 37 – 49
Edited by N. Gopalswamy, S. S. Hasan, P. B. Rao and Prasad Subramanian

Coronal mass ejections and space weather

David F. Webb*

Institute for Scientific Research, Boston College, 140 Commonwealth Ave., Chestnut Hill, MA 02457, U.S.A.

Abstract. Severe space weather effects can cause spacecraft damage and orbit degradation, increases of radiation dosage to people on aircraft and to astronauts, and damage to power lines and power stations. Such effects are usually associated with geomagnetic storms, the largest of which are driven by coronal mass ejections (CMEs). CMEs are typically observed in white light near the Sun by coronagraphs, recently the SOHO LASCO and the STEREO SECCHI CORs. In the last decade two heliospheric imagers have added wide-field viewing capabilities of CMEs in the heliosphere, the Solar Mass Ejection Imager (SMEI) in Earth orbit and the STEREO Heliospheric Imagers (HIs) in 1 AU solar orbits. Many CMEs have now been observed by these instruments and their signatures detected in–situ at Earth/L1 and/or by one or both STEREO spacecrafts. Other highlights include the following. During the last extended minimum, solar activity was very low and geostorm activity was the lowest in the last 80 years. The linear relationship between CME and sunspot rates has been maintained for 4 solar cycles, although there is evidence that the rates are diverging during the current cycle, possibly related to weak polar fields. Recent near-real time arrival-time predictions for several CMEs demonstrate that combinations of LASCO, STEREO and SMEI data can significantly improve forecasts. In the last decade heliospheric imager data have been used for 3-D CME reconstructions to study their propagation and kinematics and to improve our knowledge of space weather, but no new Earth-based instruments are planned.

Keywords : coronal mass ejections – space weather – magnetic clouds

*email: david.webb@bc.edu

1. Introduction

Coronal mass ejections (CMEs) consist of large structures containing plasma and magnetic fields that are expelled from the Sun into the heliosphere. They are of interest, scientifically because they remove built-up magnetic energy and plasma from the solar corona, and, technologically, because they drive the most extreme space weather effects at Earth, as well as at other locations throughout the heliosphere. The CME plasma is entrained on expanding magnetic field lines which can be helical with changing pitch angles, suggesting a flux rope. I review the best-determined coronal properties of CMEs, key signatures of CMEs in the solar wind, and how they drive space weather. I conclude with more recent observations of the propagation of such transients from the Sun through the heliosphere.

Until recently, images of CMEs have been made near the Sun primarily by coronagraphs on board spacecraft. Coronagraphs view density structures by imaging Thomson-scattered sunlight from the free electrons in coronal and heliospheric plasma. This emission has an angular dependence which must be accounted for in the measured brightness (e.g., Howard & Tappin 2009). CMEs are faint relative to the background corona but dynamic, so some form of background subtraction is typically used to identify them by their excess brightness and motion. Coronagraph observations of CMEs have been made from OSO–7 (early 1970s), Skylab (1973–1974), P78–1 (Solwind) (1979–1985), and SMM (1980; 1984–1989). In late 1995, SOHO was launched and two of its three LASCO coronagraphs are still operating (Brueckner et al. 1995), and have detected well over 10^4 CMEs during their lifetime (Gopalswamy et al. 2009b). Late in 2006, LASCO was joined by the STEREO CORs (Howard et al. 2008). These spaceborne observations have been complemented by white light data from the ground-based Mauna Loa Solar Observatory (MLSO) K-coronameter. During the early years interplanetary (IP) transients, at larger distances from the Sun, were observed using IP radio scintillation (IPS; Hewish et al. 1964) and from the zodiacal light photometers on the twin Helios spacecraft (Jackson 1985). The Helios photometers observed the inner heliosphere from 0.3–1.0 AU but with a limited field of view. In the past decade a new class of detector, the heliospheric imager, was developed with the first, the Solar Mass Ejection Imager (SMEI), launched on board *Coriolis* in 2003. The Heliospheric Imagers (HIs) on the twin STEREO spacecraft were launched in late 2006. SMEI observed nearly 400 transients during its 8.5 year lifetime (e.g., Webb et al. 2006) until switched off in September 2011.

2. Comparison of solar and geo-activity

Earth's geomagnetic activity tends to follow the solar sunspot, or activity cycle. The overall correspondence between the sunspot and geoactivity cycles can be seen in long-term plots comparing indices of the two kinds of activity. Fig. 1a compares the annual numbers of sunspots and the geoindex, Ap, showing that the geoactivity cycle has more structure than the solar cycle, but does tend to track sunspots. The figure also illustrates the double-peaked nature of the geoactivity cycle, with a peak near sunspot maximum and another often higher peak during the declining phase. The two main peaks represent the maximum phases of two components of geoactivity with different solar and heliospheric sources: the first associated with CMEs that track the solar cycle in amplitude and phase, and the later peak with recurrent high speed wind streams from coronal holes.

Richardson et al. (2002) studied the relative contributions of different types of solar wind structures to the *aa* index from 1972–2000, and Richardson & Cane (2012) updated the study using other geoindices through 2011. They identified CME-related flows, corotating high-speed streams, and slow flows near Earth, finding that each type contributed significantly to *aa* at all phases of the cycle. For example, CMEs contribute $\sim$ 50% of *aa* at solar maximum and $\sim$ 10% at minimum, whereas high speed streams contribute $\sim$ 70% at minimum and $\sim$ 30% at maximum. This is illustrated for the last four solar cycles in Fig. 1b. This compares the SSN with the annual numbers of small, medium, and large geostorms according to their solar wind sources. CMEs are responsible for the largest storms, which peak at solar maximum, and corotating streams drive the smaller storms, peaking during the declining phase. Note that, in concert with the general low level of activity during the last minimum, geostorm activity was the lowest in the last 80 years.

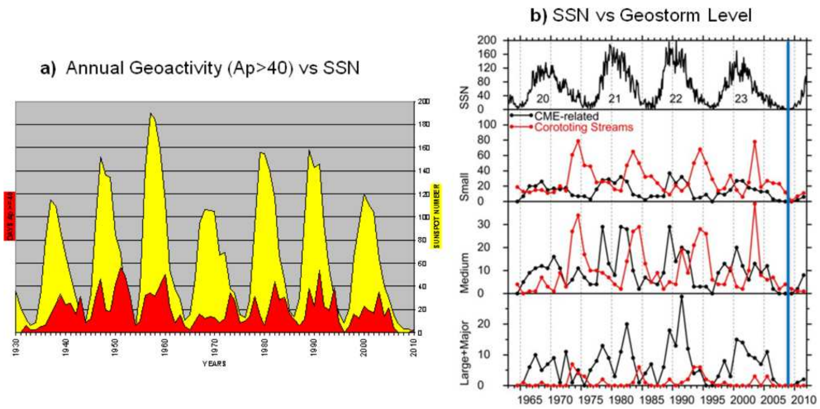

Figure 1. Solar vs Geo-activity. (a) SSN (light; yellow) and the geoactivity index, Ap, for days with $Ap > 40$ (dark; red) over last seven solar cycles. Courtesy J. Allen, NDGC. (b) Plot of last four solar cycles comparing, top to bottom, the SSN with the annual numbers of small, medium and large storms according to their solar wind sources: CMEs (black) or CIRs (red). Vertical line denotes time of last solar minimum. From Richardson & Cane (2012).

3. Importance and properties of CMEs

The driving forces of CMEs are not well understood, but related to solar magnetic fields, which help push the coronal material out of solar gravitational potential well.

The driving can continue well into heliosphere (~0.5 AU). CMEs are also one of the three ways in which mass is expelled from the Sun, the other two being the solar wind itself and solar energetic particles (SEPs). CMEs represent the most energetic phenomenon in heliospace and drive most major geomagnetic storms. Fast CMEs drive shocks that can accelerate electrons and ions producing solar energetic particle (SEP) events (Gopalswamy et al. 2008).

The measured properties of CMEs include their occurrence rates, locations relative to the solar disk, angular widths, speeds and accelerations, masses and energies. There is a large range in the basic properties of CMEs, although some of this scatter is likely due to imaging projection effects (e.g., Cremades & Bothmer 2004). Their speeds, accelerations, masses and energies extend over 2–3 orders of magnitude. CMEs can exhibit a variety of forms, some having the classical "three-part" structure, usually interpreted as compressed plasma ahead of a flux rope followed by a cavity surrounded by a bright filament/prominence (Fig. 2).

Because of their increased sensitivity, field of view and dynamic range, the SOHO-/LASCO and STEREO/COR coronagraphs now often observe halo CMEs, which appear as expanding, circular brightenings that completely surround the coronagraphs' occulting disks. Observations of associated solar disk activity helps distinguish whether a halo CME was launched from the front or backside of the Sun relative to the observer. Partial and full halo CMEs occur at a rate of about 10% that of all CMEs, but full halos are only detected at a rate of ~4% of all CMEs. The population of halo CMEs is faster and more energetic than non-halo CMEs (e.g., Gopalswamy et al. 2010a). Halo CMEs are important for three reasons: (1) The source regions of frontside halo CMEs can be studied in greater detail than for most CMEs which are observed nearer the limb. Since 2007 many CMEs have been observed by the "three eyes" of STEREO-B, LASCO and STEREO-A from different viewpoints, thus reducing projection effects. (2) If propagation effects are minimal, the internal material of CMEs can be sampled in–situ at the spacecraft along the Sun–spacecraft line. (3) When Earth-directed, halo CMEs are the key link to major space weather phenomena such as geomagnetic storms and SEPs. The vast majority of intense geomagnetic storms of Cycle 23, e.g., were caused by halo CMEs (Gopalswamy et al. 2010a).

In the past CMEs were identified by visual inspection of coronagraph images, and many of these "manual" catalogs of CMEs observed by the P78/Solwind, SMM C/P, and LASCO C2 and C3 coronagraphs (e.g., Gopalswamy et al. 2010b) are now on-line. Recently, these catalogs have been augmented by catalogs of CMEs detected by automatic methods. One is CACTus (Robbrecht et al. 2009a), which uses the Hough transform to detect motion of the brightest structures of CMEs. The SEEDS (Olmedo et al. 2008) and ARTEMIS (Boursier et al. 2009) catalogs are based on automated detection of CMEs by the LASCO C2 coronagraph. ARTEMIS detects CMEs on synoptic Carrington maps.

The frequency of occurrence of CMEs observed in white light tends to track the

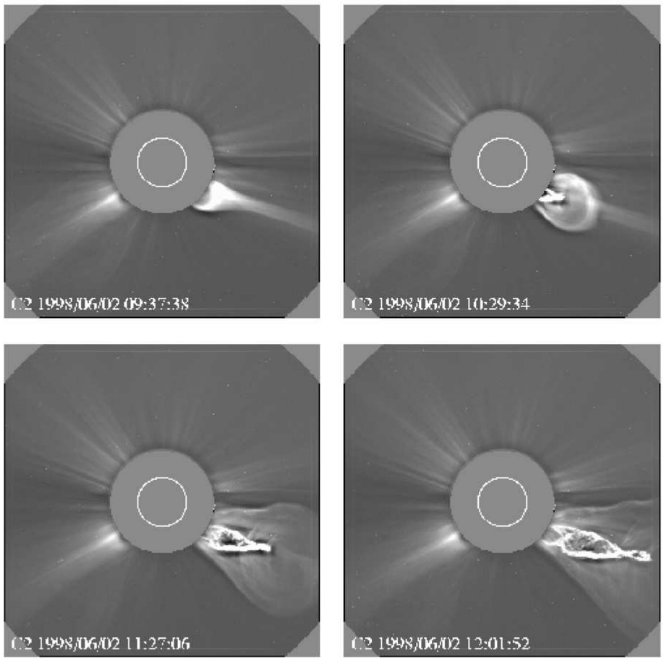

Figure 2. Evolution of a "3-part" CME observed by the LASCO C2 coronagraph on 2 June 1998. Note the circular structures just above the prominence, suggesting a flux rope. From Plunkett et al. (2000).

solar cycle in both phase and amplitude, which varies by an order of magnitude over the cycle (Webb & Howard 1994). LASCO has now observed the entire Cycle 23 (1996–2008) (Fig. 3) and continues to observe through the rise and current maximum of Cycle 24. It has detected CMEs at a rate slightly higher than earlier observations, varying from around 0.3/day around solar minimum to $\sim$ 4/day at maximum. The CME rate at minimum has remained relatively constant over the last four minima. Estimates of the apparent speeds of the leading edges of CMEs range from about 20 to >2500 km/s, from below the sound speed in the lower corona to above the Alfven speed. LASCO CME speeds increased with SSN in cycle 23 (St. Cyr et al. 2000; Gopalswamy 2006), from 280 km/s at solar minimum to 500 km/s near maximum (Fig. 3).

A 13-month running average of the LASCO CME rate vs. SSN shows that both had double peaks, but that the CME peak lagged sunspots by many months. This lag appears to be typical of solar cycles and is related to at least two factors. First, CMEs have two sources: active regions and quiet-region filaments. High–latitude polar crown filaments are the source of most high–latitude CMEs. The PC filaments have a "rush to the poles" near maximum and disappear (erupt) with a frequency that slightly lags SSNs at low latitudes (Cliver & Webb 1998; Gopalswamy et al. 2003). The other factor is that the solar activity rate differs between the hemispheres, with the activity and polarity reversal of one hemisphere usually leading or lagging the other by ~6 months to 1.5 years. For example, plots of the north-south distribution of SSNs over the last few cycles show that the northern hemisphere has dominated during the rises to first maximum whereas the south has dominated from the second maximum through the declining phases. Currently the north is dominating during the rise of cycle 24.

As has been well documented, Cycle 23 lasted ~13 years with an unusually long decline and flat minimum with its base in late 2008. With the STEREO data and the automatic catalogs, we now have six independent (white light) CME rates from 2007 to the present. Despite differences in amplitude, the CME rate has continued to track the SSN through its minimum over the last several cycles. The linear relationship between CME rate and SSNs was first estimated for Skylab by Hildner et al. (1976) and more completely for cycles 20 –22 by Webb & Howard (1994). Their value was recently confirmed for Cycle 23 by Robbrecht et al. (2009a). However, some variations over a solar cycle have been found (Gopalswamy et al. 2010a) and, since 2011, the CME rate appears to be diverging from the SSN, possibly related to the weakness of the cycle 23 –24 polar fields (e.g., Petrie 2013).

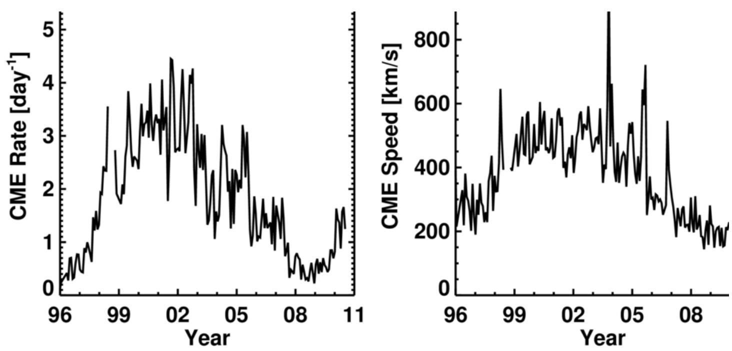

Figure 3. LASCO CME occurrence rate (left) and mean speed (right) from 1996 to 2011 averaged over Carrington rotations. Modified from Gopalswamy et al. 2010a (updated S. Yashiro, priv. comm. 2011).

The latitude distribution of the central position angles of CMEs tends to cluster about the equator at solar minimum but broadens over all latitudes near solar maximum. Hundhausen (1993) first noted that this CME latitude variation more closely parallels that of streamers and prominences than of active regions or sunspots. This pattern is linked to the variation of the global magnetic field, as exemplified by the tilt angle of the HCS when the Sun transitions between solar minimum and maximum. This pattern including the match between CMEs, prominence eruptions and the HCS has been confirmed with the LASCO data (Gopalswamy et al. 2004; 2010b).

4. Interplanetary CMEs and geostorms

The coronal magnetic fields and plasma that CMEs carry into the heliosphere can be detected by remote sensing and in-situ spacecraft observations. There they had been called IP CMEs or ICMEs, but now that CMEs can be tracked continuously from the Sun to 1 AU and beyond, the term has become redundant. CME material passing a single spacecraft has distinctive signatures, but with a large amount of variation (e.g., Gosling 1993). These signatures include transient IP shocks, depressed proton temperatures, cosmic ray depressions, flows with enhanced helium abundances, unusual compositions of ions and elements, and magnetic field structures consistent with looplike topologies. Although the outline of a CME is visible near the Sun because it is denser than the ambient solar wind, its expansion often produces lower densities farther from the Sun. Many of these signatures were first identified in the plasma following an IP shock and, thus, was considered to be the piston driving the shock. Some signatures can also be observed elsewhere in the solar wind where they may identify relatively slower CMEs not driving shocks.

Highly structured magnetic field configurations can signal the arrival of a CME. The magnetic field can be helical and/or rotational, and is accompanied by other signatures including strong fields with low variance, low plasma beta and low temperature. Such structures were called magnetic clouds by Burlaga et al. (1981), citing early theoretical work dating back to the 1950s (Morrison 1954). Since many if not all CMEs are now considered to contain flux ropes, it is logical to expect magnetic clouds to form the core of CMEs (Gopalswamy 2013). Recently, one magnetic cloud observed in–situ was tracked continuously back to its coronal origin as the cavity in a three-part CME structure (Howard & DeForest 2012). Models have been developed for the force free (e.g., Lepping, Burlaga & Jones 1990; Lynch et al. 2005) and non-force free (Hu & Sonnerup 2001) states of magnetic clouds observed in–situ. Around 30–50% of CMEs observed in–situ can clearly be associated with magnetic clouds. It remains unknown whether the remainder does not show the signature because the imbedded flux rope is less structured, absent or the spacecraft did not pass through the flux rope component.

IP propagation effects can affect a CME as it travels from the Sun through the heliosphere. Such effects are particularly important near the Sun and within $\sim$1 AU. Field line reconnection is clearly important as the CME erupts through the Alfven sphere. Field line reconnection and the formation of current sheets can develop and help to reclose the fields near the surface. Interchange reconnection can open some CME field lines, eventually leading to open field lines embedded in closed fields as first shown by Gosling, Birn & Hesse (1995). CMEs can also interact with each other, in which a faster CME overtakes a slower one near the Sun, producing a collision (Gopalswamy et al. 2001). Sequential eruptions and interactions can produce so–called compound or complex ejecta at 1 AU. Such ejecta often consist of high speed flows with shocks and other CME signatures, but poorly defined magnetic structures, or "tangled fields" (e.g., Burlaga et al. 2001).

Deflections of CMEs can also occur. Isavnin, Vourlidas & Kilpua (2012) studied the deflections of 15 flux rope/magnetic clouds from 2008-2010, comparing measurements of the same magnetic clouds with coronagraphs near the Sun and Grad-Shafranov fits of clouds measured in–situ at 1 AU. Zuccarello et al. (2012) simulated an observed eruption and reproduced the equatorward deflection of a flux rope–CME towards the equator and its subsequent merger with the HCS. Some CME deflections may be caused by other CMEs or by nearby coronal holes with their strong winds and open fields (e.g., Gopalswamy et al. 2009). Rotations of CMEs have also been measured during their outward propagation. Isavnin et al. (2012) studied the rotations of CMEs comparing the near-Sun and 1 AU variations of the flux rope/magnetic clouds, finding that the CMEs tended to rotate clockwise in the inner heliosphere.

CMEs are responsible for the most geoeffective solar wind disturbances. As discussed earlier, full (360°) halo events are the most likely to be directed along the Sun-Earth line and those with frontside sources should be Earth-directed (Zhao & Webb 2003; Gopalswamy, Yashiro & Akiyama 2007). Small to moderate geostorms without CMEs are usually caused by Earth passage through the HCS and/or high speed streams and their related corotating interaction regions (CIRs). The main space weather drivers of heliospheric transient disturbances are southward IMF and compression. Southward IMF allows merging of the IMF and Earthś magnetic field and transfer of solar wind energy and mass into the magnetosphere. Compression strengthens existing southward IMF and, to a lesser extent, increases density. CMEs usually contain long-duration flows of southward IMF and fast CMEs compress any southward field ahead. Sometimes the geoeffective compressed, southward field can be entirely within the shock “sheath”. High–speed streams are geoeffective when they compress any southward IMF in CIRs, and they can drive the acceleration of electrons in the magnetosphere to hazardous levels.

Since the start of STEREO observations early in 2007, there have been many well observed events in which a CME observed leaving the Sun by one or both STEREO (SECCHI) and/or SOHO (LASCO) spacecraft passed over one of the STEREO spacecraft or at L1/Earth, so could be detected in in–situ data. From Earth, the associated activity regions on the Sun can be well observed by SOHO, Hinode and SDO instruments, and the heliospheric propagation of the CMEs can be observed by the STEREO HIs and SMEI. These events provide important information on the geometry, propagation and internal structure of CMEs. For example, we know that most of these CMEs also had magnetic cloud signatures at 1 AU. The STEREO Space Weather Group website (http://secchi.nrl.navy.mil/spwx/) catalogs these events and contains other useful STEREO space weather data and modeling links.

These Sun to STEREO/L1 data sets are also being used for forecasting space weather events. During 2010 –2011, the STEREO Group members made near-real time event predictions utilizing the STEREO Beacon data for three events: 8 –12 April 2010 (Davis et al. 2011), the 30 July – 4 August 2010 series of multiple events e.g., Harrison et al. (2012), and the 15 –18 February 2011 X –class flare–CME. The

Group predictions for these three sets of events were based on several models and techniques, here demonstrated for the February 2011 event. This was an X2.2 long–duration flare that occurred on 15 February, onset 01:44 UT, near Sun center. It had a nearly symmetrical full–halo CME observed by LASCO, suggesting it would be geoeffective. This event was the first X–class flare to occur in over 4 years.

The data and techniques/models used included geometric localization and polarization (DeKoning & Pizzo, 2011) on STEREO COR2A, B images, HI "J–plots" (Davis et al. 2011), D. Biesecker (NOAA) empirical model, the HAFv2 model (Hakamada & Akasofu 1982), the Enlil+WSA model, the STOA shock model (Dryer & Smart 1984), the Empirical Shock Arrival model (ESA – Gopalswamy et al. 2001), and the Tappin-Howard model (T–H; Tappin & Howard 2009) using HI and SMEI data. We intercompared the results of the near-real time runs of these techniques to forecast the time of Earth arrival of the 15 February CME. Both the time that the prediction was issued and the predicted time of arrival were recorded for each run. Fig. 4 is a plot of prediction accuracy vs the time the prediction was made. Predictions using primarily coronagraph data (LASCO or STEREO CORs) are in blue and those including HI data (SMEI or STEREO HIs) are in red.

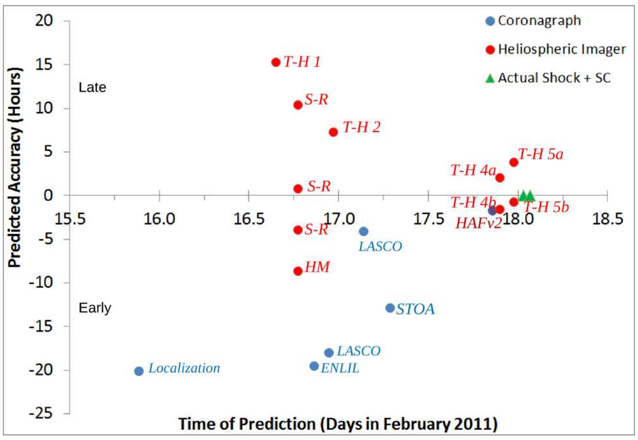

Figure 4. Example of space weather forecasting for the 15 February 2011 halo CME. Plot of prediction accuracy vs the time of prediction for the range of model runs. Prediction accuracy is defined as the [actual arrival time – predicted arrival time] where the actual AT is defined as the shock time at ACE (L1): 18 February, 00:42 UT, the first green triangle on the plot. Model predictions using coronagraph observations are in blue and those using heliospheric imager data are in red. Points lying above the horizontal 0–hour line are positive and therefore "late" and those lying below the line are negative or "early". The best predictions should be near the 0–line and near the left side, i.e, be accurate and have a long lead time.

For this event the models incorporating the HI data generally provided better forecasts. The T–H and S–R (Sheeley & Rouillard 2010) j–plot techniques using HI and/or SMEI data and the HAFv2 and ESA models using LASCO data gave the best predictions, within ±5 hours. For all three event periods, we assessed the prediction performances for a dozen techniques that were used by the STEREO Group. The accuracy averaged 8.0 hr. with a large range, a clear improvement over the typical time–of–arrival uncertainties in the past literature of 11–12 hr. The lead or warning time averaged ~1 day. Use of the STEREO and SMEI data improved performance, however, for the forecasts only the STEREO Beacon data was used, which has reduced cadence (2 hr), incomplete temporal coverage and reduced spatial resolution compared to the normal science data. Davis et al. (2011) demonstrated that the STEREO science data would have yielded better predictions, thus, a mission with imagers dedicated to space weather will provide the best performance. We note that, despite hitting the Earth with strong magnetic fields, the 15 –18 February event proved not very geoeffective. This was because the field throughout the event was almost entirely northward, which has been the case with many Earthward CMEs this cycle helping explain the small number of geostorms.

5. Imaging and tracking transients in the heliosphere

The remote sensing of CMEs at large distances from the Sun has been revolutionized in the last decade by the new class of white light HIs. Other techniques developed to remotely detect and track IP transients include kilometric radio observations from space and metric radio IP scintillation (IPS) observations from the ground.

The heritage of the current HIs is the zodiacal light photometers (Leinert et al. 1975) on the twin Helios spacecraft flown in solar orbits in the 1970s and 1980s. Unlike Helios, which could only observe a few narrow strips across the sky, the new generation of imager can observe large areas simultaneously. SMEI was the first, developed as a proof-of-concept U.S. Air Force experiment to detect and track CMEs for operational forecasting. Launched in 2003 on the *Coriolis* spacecraft, SMEI imaged nearly the entire sky in white light once per 102–minute spacecraft orbit, using three baffled camera systems. SMEI over its 8.5 year lifetime observed about 50 CMEs that were Earth–directed (e.g., Howard et al. 2006; Webb et al. 2009), allowing comparisons with in–situ spacecraft and prediction of arrival times and speeds. SMEI could detect and track CMEs 10 hr to or so a day before Earth arrival, and could also detect the auroral light associated with the subsequent storms (see Howard et al. 2013).

A new processing pipeline using SECCHI data has been developed that minimizes many sources of noise (starfield, F corona, etc.). This has permitted the tracking and measurement of features previously inaccessible. Analyses of these data are just beginning, but early results include observations and measurements of CME structure (DeForest, Howard & McComas 2013), CME flux ropes (Howard & DeForest 2012), and disconnection events (DeForest, Howard & McComas 2012). U- or V-shaped features in processed SECCHI/HI-2 images are considered a sign of magnetic disconnection. For an event on 18 December 2008, DeForest et al. (2012) found a surprising increase in the accreted mass of a factor of 4 over the 1 AU distance, likely due to the structure "snowplowing" and compressing solar wind material ahead of it. DeForest et al. also estimated the entrained magnetic field by balancing the magnetic tension force to drag and found 0.08 G at 7 R_S. This value can be compared to recent results using white light coronagraph CME and shock data; e.g., Gopalswamy & Yashiro (2011) and Poomvises et al. (2012). Such events are not uncommon even during this period at solar minimum. Over a 36–day period they found 12 events and calculated a disconnection rate of the unsigned flux of 6×10^{21} Mx/yr. This corresponds to a change in the radial IMF at Earth of 0.2 nT/yr., or about 10% of the observed rate of change of the open magnetic field at 1 AU (e.g., Schwadron et al. 2010). Therefore, they conclude that CMEs may play an important role in balancing the open flux in the heliosphere.

Currently two HI instruments are being designed and built by consortia led by the Naval Research Lab: WISPR on Solar Probe and SolOHI on Solar Orbiter. They are of similar design based on the STEREO SECCHI HIs, shoebox-type structures with simple lens systems buried deep in baffles to minimize stray light from the sky and other spacecraft structures. WISPR will view from 13.5–118° and SOLOHI from 5.5–45° from the Sun. They both record broadband visible light and use next-generation 2k x 2k APS sensors. Both imagers will image the fine–scale structure of the solar wind, and provide observations to acquire density power spectra and look at density turbulence as a function of heliocentric distance.

Other opportunities are being examined for future HI instruments for operational or research capabilities. An Earth orbit remains a lower cost option, but any instrument in Earth orbit suffers from radiation damage and penetrating trapped particles. Those in low Earth orbit (LEO) passing through the South Atlantic Anomaly or auroral zones suffer from particle effects and/or bright auroral emission. In a LEO, near-equatorial orbit, this contamination is reduced; other Earth orbits such as medium Earth orbit (MEO) are possible. In deep space, an L1 halo orbit is probably easiest to reach, however, imagers there cannot directly observe the most geoeffective part of Earthward (halo) CMEs because of the need to occult bright sunlight. Imagers at the 4th and 5th Sun-Earth Lagrange points will be able to measure CME speed and direction for a range of solar origin locations. An instrument at L5 has the advantage of viewing beyond the solar Earth-facing east limb. Thus, active regions and coronal holes can be viewed before they arrive on the Earth-facing disk, and their location, size and activity assessed. Finally, the geoeffective space weather resulting from high–speed solar wind streams can be forecast days in advance. Using STEREO–B as a pathfinder for such a mission was discussed by Webb et al. (2010), and an L5 mission called EASCO is described in Gopalswamy et al. (2011). In addition, an L5 mission with heliospheric imagers is included in the recent Solar and Space Physics Decadal Survey.

Heliospheric imager data now are being used to produce 3-D reconstructions of CMEs to study their propagation through the inner heliosphere and to improve our knowledge of space weather. However, soon there will be no operating HIs capable of making space weather measurements, because SMEI has been turned off and the STEREOs will be too distant, and the SOHO spacecraft is well beyond its design lifetime. Thus, new coronagraphs and HIs are needed to observe and study transients and improve our forecasting of space weather.

Acknowledgements

We thank N. Gopalswamy, S. Yashiro, A. Vourlidas, T. Howard and C. DeForest for providing material for this article. We benefitted from data from the SOHO and STEREO missions, both international collaborations between NASA and ESA. We also used the SOHO/LASCO CME catalog, maintained by The Catholic University of America in cooperation with the Naval Research Laboratory (NRL) and NASA. The Solar Mass Ejection Imager (SMEI) instrument is a collaborative project of the U.S. Air Force Research Laboratory, NASA and several universities. The STEREO SECCHI project is an international consortium led by NRL. This work was supported at Boston College by NASA STEREO grant NOO173-10-1-G001.

References

Boursier Y., Lamy P., Llebaria A., Goudail F., Robelus S., 2009, Solar Phys., 257, 125
Brueckner G.E., et al., 1995, Solar Phys., 162, 357
Burlaga F., Sittler E., Mariani F., Schwenn R., 1981, JGR, 86, 6673
Burlaga L.F., Skoug R.M., Smith C.W., Webb D.F., Zurbuchen T.H., Reinard A., JGR, 2001, 106, 20,957
Cliver E.W., Webb D.F., 1998, in IAU Colloq. 167: New Perspectives on Solar Prominences, (Eds.) Webb, D.F., Schmieder, B., Rust, D.M., vol. 150 ASP Conference Series, p. 479, Astronomical Society of the Pacific, San Francisco.
Cremades H., Bothmer V., 2004, A&A, 422, 307
Davis C. et al., 2011, Space Weather, 9, S01005
DeForest C.E., Howard T.A., McComas D.J., 2012, ApJ, 745, 36
DeForest C.E., Howard T.A., McComas D.J., 2013, ApJ, in press
De Koning C.A., Pizzo V.J., 2011, Space Weather, 9, S03001, doi:10.1029/2010SW000595
Dryer M., Smart D.F., 1984, Adv. Space Res., 4, 291
Gopalswamy N., 2006, Space Sci. Rev., 124, 145
Gopalswamy N., 2013, BASI, in press
Gopalswamy N., Yashiro S., 2011, ApJ, 736, L17
Gopalswamy N., Lara A., Yashiro S., Kaiser M., Howard R. A., 2001, JGR, 106, 29,207
Gopalswamy N., Shimojo M., Yashiro S., Howard R.A., 2003, ApJ., 586, 562
Gopalswamy N., Shimojo M., Lu W., Yashiro S., Shibasaki K., Howard R.A., 2004, Adv. Space Res., 33, 676
Gopalswamy N., Yashiro S., Akiyama S., 2007, JGR, 112, A06112
Gopalswamy N., Yashiro S., Akiyama S., Makela P., Xie H., Kaiser M.L., Howard R.A., Bougeret J.–L., 2008, Ann. Geophys., 26, 1
Gopalswamy N., Makela P., Xie H., Akiyama S., Yashiro S., 2009a, JGR, 114, A00A22
Gopalswamy N., Yashiro S., Michalek G., Stenborg G., Vourlidas A., Freeland S., Howard R., 2009b, Earth Moon Planets, 104, 295

Gopalswamy N., Akiyama S., Yashiro S., Makela P., 2010a, in Hasan S.S., Rutten R.J., Eds, Magnetic Coupling between the Interior and the Atmosphere of the Sun, Astrophysics and Space Science Proceedings, p. 289, Springer, Heidelberg; Berlin
Gopalswamy N., Yashiro S., Michalek G., Xie H., Makela P., Vourlidas A., Howard R.A., 2010b, Sun and Geosphere, 5, 7
Gopalswamy N., Davila J. M., St. Cyr O. C., et al. 2011, JASTP, 73, 658
Gosling J.T., 1993, JGR, 98, 18,937
Gosling J. T., Birn J., Hesse, M., 1995, GRL, 22, 869
Hakamada K., Akasofu S.-I., 1982, Space Sci. Rev., 31, 3
Harrison R. et al., 2012, ApJ, 750, 45
Hewish A., Scott P.F., Wills D., 1964, Nature, 203, 1214
Hildner E., Gosling J. T., MacQueen R. M., Munro R. H., Poland A. I., Ross C. L., 1976, Solar Phys., 48, 127
Howard T. A., DeForest C.E., 2012, ApJ., 746, 64
Howard T. A., Simnett G.M., 2008, JGR, 113, A08102
Howard T. A., Tappin S.J., 2009, Space Sci. Rev., 147, 31
Howard T. A., Webb D.F., Tappin S.J., Mizuno D.R., Johnston J.C., 2006, JGR, 111, A12101
Howard R. A. et al., 2008, Space Sci. Rev., 136, 67
Howard T. A. et al., 2013, Space Sci. Rev., 180, 1
Hu Q., Sonnerup B. U. O., 2001, GRL, 28, 467
Hundhausen A. J., 1993, JGR, 98, 13,177
Isavnin A., Vourlidas A., Kilpua E. K. J., 2012, Solar Phys, DOI 10.1007/s11207-012-0214-3
Jackson B. V., 1985, Solar Phys., 100, 563
Leinert C., Link H., Pitz E., Salm N., Knueppelberg D., 1975, Raumfahrtforschung, 19, 264
Lepping R. P., Burlaga L. F., Jones J. A., 1990, JGR, 95, 11,957
Lynch B.J., Gruesbeck J. R., Zurbuchen T. H., Antiochos S. K., 2005, JGR, 110, A08107
Morrison P., 1954, Phys. Rev., 95, 646
Olmedo O., Zhang J., Wechsler H., Poland A., Borne K., 2008, Solar Phys., 248, 485
Petrie G. J. D., 2013, ApJ, 768, 162
Plunkett S. P., Vourlidas A., Ŝimberová S., Karlickỳ M., Kotrĉ P., Heinzel P., Kupryakov Yu. A., Guo W.P., Wu S.T., 2000, Solar Phys., 194, 371
Poomvises W., Gopalswamy N., Yashiro S., Kwon R-Y, Olmedo O., 2012, ApJ, 758, 118
Richardson I., Cane H., 2012, J. Space Weather Space Clim. 2, A01, DOI: 10.1051/swsc/2012001
Richardson I. G., Cane H. V., Cliver E. W., 2002, JGR, 107, A8, doi:10.1029/2001JA000504
Robbrecht E., Berghmans D., van der Linden R. A. M., 2009a, ApJ., 691, 1222
Robbrecht E., Patsourakos S., Vourlidas A., 2009b, ApJ, 701, 283
Schwadron N.A., Connick D. E., Smith C., 2010, ApJ, 722, L132
Sheeley Jr, N. R., Rouillard A. P., 2010, ApJ., 715, 300
St Cyr O. C. et al., 2000, JGR, 105, 18,169
Tappin S. J., Howard T. A., 2009, Space Sci. Rev., 147, 55
Webb D. F., Howard R. A., 1994, JGR, 99, 4201
Webb D. F. et al., 2006, JGR, 111, A12101
Webb D. F., Howard T. A., Fry C. D., Kuchar T. A., Mizuno D. R., Johnston J. C., Jackson B. V., 2009, Space Weather, 7, S05002
Webb D. F. et al., 2010, Space Res. Today, 178, 10
Zhao X. P., Webb D. F., 2003, JGR, 108, 1234, doi:10.1029/2002JA009606
Zuccarello F. P., Bemporad A., Jacobs C., et al., 2012, ApJ, 744, 66